Geomechanics for Energy and the Environment 38 (2024) 100508

Contents lists available at ScienceDirect

Geomechanics for Energy and the Environment

journal homepage: www.elsevier.com/locate/gete

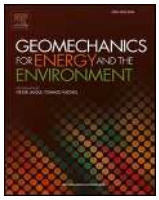

Insights from an extensive triaxial testing campaign on a shale for comparative site characterization of a deep geological repository

E. Crisci [a,*], S.B. Giger [b], L. Laloui [c], A. Ferrari [c,d], R. Ewy [e], R. Stankovic [f], J. Stenebråten [g], K. Halvorsen [h], M. Soldal [h]

[a] Nesol, Numerical Engineering Solutions, Lausanne, Switzerland
[b] National Cooperative for the Disposal of Radioactive Waste (NAGRA), Wettingen, Switzerland
[c] Ecole Polytechnique Fédérale de Lausanne, EPFL, Lausanne, Switzerland
[d] University of Palermo, Engineering Department, Palermo, Italy
[e] Tufts University, MA, USA
[f] RSTD, UT, USA
[g] Sintef, Trondheim, Norway
[h] NGI, Oslo, Norway

ARTICLE INFO

Keywords:
Geological storage
Opalinus clay
Shale testing
Triaxial tests

ABSTRACT

Several boreholes were drilled for site comparison of a deep geological repository (DGR) in Northern Switzerland. The main target of the exploration program was the >100m thick Opalinus Clay, the designated host rock encountered at approximately 450 to 1000 m depth in three different sites. This contribution focuses on the evaluation of geomechanical properties and the deformation behavior from the triaxial testing campaign, both aspects relevant to construction and the assessment of the long-term safety of a DGR. Some 140 triaxial tests were performed on cores from seven different boreholes to evaluate potential differences in material properties by depth and geographic location. Core sampling, preparation chain, and testing protocols were validated before the campaign, and three laboratories were commissioned to perform the tests. A comparison of basic properties from cores used for triaxial testing with a much larger database of complementary core analyses and geophysical logging demonstrates that the performed tests cover the range of expected material properties. Limited to no differences in strength and stiffness are detected from cores at different depths and sites. Despite a relatively large variation in bulk mineralogy of the formation (e.g. clay-mineral content varying between 35 and 75 wt%), the strength values of Opalinus Clay vary only moderately, with equivalent (calculated) unconfined compressive strengths of 21 ± 5 MPa, for loading directions parallel or perpendicular to bedding. This contrasts with the results of Opalinus Clay from the Rock Laboratory at Mont Terri, where the effect of material composition was more relevant. Assuming a Mohr-Coulomb-type failure law, the transition from peak to post-peak strength comes at the expense of cohesion, and only a small reduction of the shear strength angle. Hence the burial history, tectonic overprint, and current depth mainly control the intact properties by additional cohesion, whereas the post-peak behavior is mainly controlled by bulk mineralogy.

1. Introduction

Shales are geomaterials involved in several engineering applications related to extraction from, and storage in, the underground. Examples include the production of oil and gas from unconventional reservoirs, underground gas storage (e.g., carbon dioxide, hydrogen), and the disposal of radioactive waste.

Testing of shales in the laboratory proved challenging because of their very small pore sizes (tens of nanometres) leading to low permeabilities (nanodarcies or lower). The main difficulty arises from measuring and keeping the pore pressure equilibrium to correctly evaluate the effective stress acting on the specimen throughout the test. Pore pressure control needs an accurate loading rate, which is usually very low, and extends the time of testing from hours or days, as typical for rocks, to weeks or even months[7,18]. Neglecting this aspect can cause a relevant over (or under) estimation of the mechanical parameters[10].

* Corresponding author.
E-mail address: eleonora.crisci@nesol.net (E. Crisci).

https://doi.org/10.1016/j.gete.2023.100508
Received 8 September 2023; Accepted 29 September 2023
Available online 22 January 2024

In the context of the site selection for a deep geological repository for radioactive waste in Switzerland, nine "deep" boreholes (TBO) were drilled between the years 2019 and 2022 in the northern part of the country. The convention name "deep boreholes" is used here to align with the terminology of the deep geological repository, and to highlight greater depths (in the order of of 1000 m) than what is standard in geotechnical investigations. The main aim of these boreholes was to characterize the barrier properties of the designated host rock, the Opalinus Clay shale, and its confining units, and allow for comparison among sites. Up to the present campaign, published triaxial testing results of Opalinus Clay come mainly from cores taken at the Mont Terri Underground Rock Laboratory in the Jura Mountains (Switzerland), and from earlier boreholes in the North Western and the North Eastern part of the country (e.g., [1,8,10,18,26]).

In the TBO campaign, most Mesozoic sections were cored in all boreholes, including the 100 to 120 m thick Opalinus Clay. The core material was investigated in detail, focusing on sedimentological, geochemical, mineralogical, hydrological, and geomechanical properties.

This study focuses on the geomechanical characterization of Opalinus Clay, and more specifically on the triaxial testing campaign. Part of the test results shown here is used for calibrating tunnel excavation models at the target repository depth[21].

To address the above-mentioned challenges of testing, tailor-made testing protocols were established [8,10] and assessed by round-robin comparison before the start of the large testing campaign[18].

Through complementary core analyses from other disciplines, the variability of basic material properties such as water content, bulk density, and bulk mineralogy was determined at a very high frequency in the formation (every two to five meters) and for every tested interval used for triaxial testing. This enables a unique opportunity to assess how representative the triaxial test results are for the entire formation.

In total, three laboratories (hereafter Lab A, B, and C) performed over 140 triaxial tests on Opalinus Clay core material, sourced from seven of the nine deep boreholes. The cumulative rig time if tests were done with one testing equipment, would correspond to more than seven years of testing. To the authors' knowledge, this is the most extensive coordinated triaxial testing campaign ever done with a shale.

2. Material description and testing methodology

2.1. Opalinus Clay at different sites

Three siting regions are being appraised in Switzerland's Sectoral Plan for Deep Geological Repositories (Jura Ost, Nördlich Lägern, and Zürich Nordost, Fig. 1). All three sites have Opalinus Clay as the host

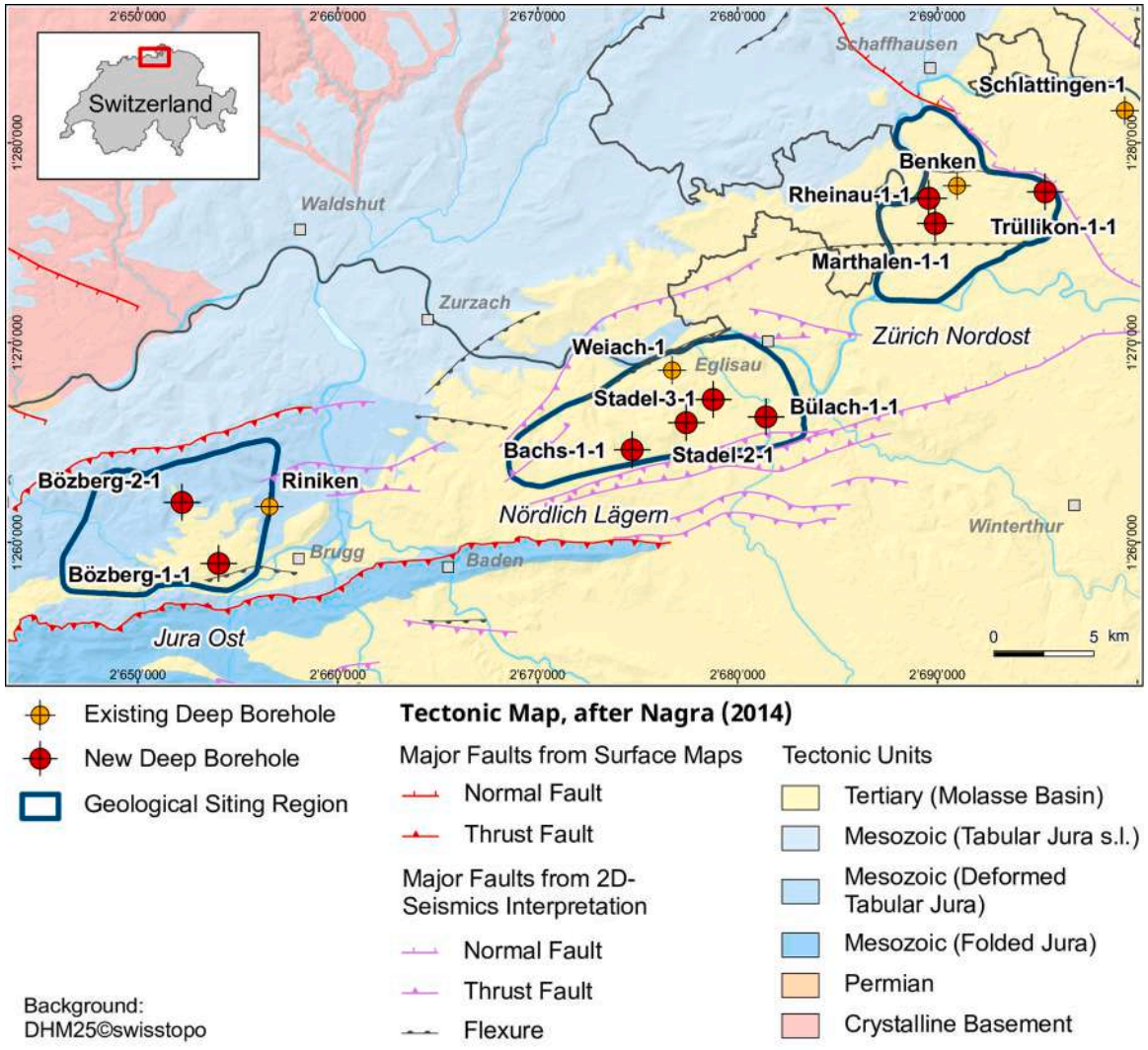

Fig. 1. Tectonic map of the three candidate sites and overview of new exploration data.

rock, but an important difference between the sites is the depth at which the host rock is encountered (Table 1).

In northern Switzerland, Opalinus Clay consists of fine-grained, silty to sandy claystone, originating from continental weathering and erosion products (clay minerals, quartz, and feldspar), marine carbonates, and diagenetic contributions (pyrite, siderite, calcite-cement, and dolomite)[16]. Bulk mineralogy was tested by XRD analysis on the geomechanically tested samples of Opalinus Clay. While within each borehole the composition varies slightly, the average composition is fairly constant across different boreholes and sites (clay mineral content reported in Table 1). The thickness of Opalinus Clay is also quite constant, varying between 104 and 122 m in the seven boreholes (Table 1). Table 1 reports the measured bulk density and water content, and the calculated porosity (assuming solid density 2.7 g/cm^3) for the geomechanically tested samples, specifying the (i) average value, (ii) observed range, and (iii) the number of observations. The results did not show any relevant difference among the three investigated sites. On the other hand, slightly higher average porosity and water content were observed in the material from the borehole MAR1–1, and to some extent also in BOZ2–1 and BOZ1–1. In these three boreholes, the formation is at a shallower current depth (452 to 705 m) compared to the other boreholes (779 to 996 m).

Opalinus Clay formed in a shallow epicontinental sea during the early Middle Jurassic period[25]. After deposition, it experienced a complex burial history[14]. The basin was subsiding in the early Cretaceous, followed by uplift and ca. 600–700 m of erosion of Late Jurassic and Cretaceous sediments in the early Paleogene. During the Paleogene the wedge-shaped Molasse Foreland Basin developed and led to another substantial burial of the Opalinus Clay with a maximum burial of approximately 1500 to 2000 m in the Miocene, followed by an uplift to present depths.

Based on existing evidence[14] and the close proximity of the three sites (Fig. 1) it can be assumed that the burial history (including maximum burial depth) of Opalinus Clay is similar in all three sites. In contrast to bulk mineralogy and burial history, the tectonic history appears quite different in the three sites, especially the increasing north-south shortening in Miocene times[20]. Yet, the Opalinus Clay shale in all three sites exhibits macroscopically mostly undeformed or weakly deformed core intervals. Since the burial history is similar among sites and the tectonic overprint is weak, potential differences in basic and geomechanical properties in the three sites are therefore expected to be related to the current burial depth.

2.2. Core handling and specimen preparation

Cores designated for geomechanical analyses (hereafter referred to as GM cores) represented one of nine major categories sampled from Opalinus Clay at each borehole. All of these categories had special requirements to minimize potential effects on laboratory analyses, and hence special conditioning methods. For the GM cores, the target exposure time to the atmosphere was set to 20 min to allow geological description and documentation (including a core scanner for photographic description). The cores were then immediately inserted into PVC tubes and axially constrained with bar clamps. The annulus was then filled with epoxy (Sikadur-52). The annulus between the core and the PVC tube was chosen to be small (nominal 3.2 mm) to ensure that the temperature rise from the curing of the epoxy was well below the in-situ temperature from which the core was sourced. Further details of the conditioning procedure are provided in the field manual[22].

To evaluate core integrity before shipping to the testing laboratories, all GM cores from Opalinus Clay and its confining units were analyzed using medical X-ray computer tomography (XCT). Details of the applied XCT method can be found in ref.[12].

Sedimentary geomaterials typically display transversely isotropic mechanical properties which are related to the orientation of the bedding. To study this anisotropic response, cylindrical specimens were tested in three orientations with respect to bedding. Most of the tests were done by axially loading perpendicular to the cylinder axis (S-specimens) and parallel to the cylinder axis (P-specimens). Additional tests were done with the cylinder axis at an angle with respect to bedding (Z-specimens). These were generally cut with an angle of 30° between the axis cylinder and the bedding direction, with the intent of obtaining the shear band formed during the shearing phase along the bedding direction, i.e. the orientation with the expected minimum strength.

The specimens' extraction was carefully performed to minimize water content loss during the operation. All involved laboratories used a rotary core barrel and hydrocarbons as cooling fluids during the drilling of the specimens. Once prepared, the specimens were either tested right away or stored submerged in oil (or in a controlled humidity chamber) to minimize evaporative water loss.

Specimens' size for testing was either 25 mm in diameter and 50 mm in length (Laboratories A and B) or 19 mm in diameter and 38 mm in length (Laboratory C).

2.3. Testing program and methodology

The determination of robust hydromechanical characterization of

Table 1
Boreholes, depth and thickness of the formation, mineralogy and basic properties of the geomechanically tested samples of Opalinus Clay in the three sites. Data reports the average value, the observed range, and the number of data points (in parenthesis). [1]Porosity is calculated from water-loss to constant weight at 105 °C, bulk wet density and assuming solid density 2.7 g/cm^3.

Site		Jura Ost (JO)		Nördich Lägern (NL)			Zürich Nordost (ZNO)	
Borehole		BOZ1-1	BOZ2-1	STA2-1	STA3-1	BUL1-1	MAR1-1	TRU1-1
Opalinus Clay	Top (mbg)	530.3	451.5	799.7	779.3	891.7	590.35	816.4
	Base (mbg)	651.4	573.7	905.2	887.9	995.9	705.40	927.9
	Thickness (m)	121.1	122.2	105.5	108.6	104.2	115.05	111.5
Bulk density (g/cm^3)		2.52	2.52	2.53	2.52	2.53	2.50	2.53
		2.48-2.56	2.48-2.55	2.49-2.59	2.50-2.54	2.46-2.58	2.46-2.52	2.49-2.55
		(21)	(18)	(12)	(13)	(31)	(19)	(29)
Water content (wt%)		4.8	5.1	4.4	4.6	4.6	5.4	4.7
		4.4-5.6	4.2-6.5	3.1-5.4	3.6-5.3	3.2-5.6	4.5-6.5	3.9-5.2
		(21)	(18)	(12)	(13)	(31)	(19)	(29)
[1]Porosity (%)		11.2	11.4	10.2	10.7	10.3	12.2	10.6
		9.4-13.0	9.3-13.6	7.1-12.0	9.4-11.5	7.4-13.5	10.6-13.8	9.5-11.9
		(21)	(18)	(12)	(13)	(31)	(19)	(29)
Clay mineral content (wt%)		55.0	59.3	50.9	59.3	50.5	58.2	56
		45.5-61.4	46.2-71.6	32.0-66.4	52.0-63.8	33.0-65.0	48.0-66.6	52-63.7
		(21)	(18)	(12)	(13)	(31)	(19)	(29)

Opalinus Clay requires triaxial tests with sound procedures and reliable measurements of the pore pressure evolution throughout the tests.

In the Opalinus Clay section and the immediate confining units, specialized protocols combining rock-mechanical and soil-mechanical best practices were adopted. Specifically, these protocols account for i) the low-permeability and fluid-sensitivity of Opalinus Clay and its argillaceous confining units, and ii) for the greater relevance of these units for construction and evaluation of the safety of a future repository.

Two testing procedures for triaxial testing (hereafter named "conventional" and "alternative" procedures) were validated in a benchmarking study[19,18], and adopted in this study.

The so-called "conventional" testing procedure foresaw the specimen resaturation in the triaxial cell at constant volume to minimize specimen disturbance (i.e. "swelling"): after vacuuming the pore lines, axial and radial stresses are progressively increased to keep the specimen's volume constant while it is put in contact with a fluid back pressure at a minimum of 2 MPa to dissolve possible air remaining in the tubing or in the material. This procedure allows the determination of the axial and radial swelling pressures. The confining stress is then set equal to the axial stress and the specimens' saturation is assessed by measuring the Skempton's B coefficient (B-test). Drained loading or controlled unloading of the specimen to the target consolidation effective stress (between 4 and 20 MPa) is then performed. The final stage is the shearing of the specimens at a constant axial strain rate. An unloading/reloading loop is performed, and then the shearing continues until the specimen's failure and achievement of the postpeak constant deviatoric stress, in undrained or drained conditions.

The "alternative" procedure foresees the equalization of the specimen to high relative humidity values (between 70% and 96%) in desiccators before testing to achieve high saturation conditions. After that, the specimens are mounted in the rig, and an initial undrained isostatic loading is carried out until an increase in the pore pressure is detected. At this stage, the specimen is considered to have achieved the fully saturated condition, confirmed by performing B-tests. A pressure transducer is placed inside the vessel adjacent to the specimen to monitor the evolution of the pore fluid pressure during the application of external mechanical stress. When this testing procedure is adopted, no or small amounts of artificial pore fluid are added to the specimen. Consolidation or swelling, and shearing follow the same procedure as the conventional one. A detailed description of the two procedures and the assessment of the comparability in the results is provided by ref. [18].

All sites were explored at a similar level of detail to allow comparisons among sites. To account for the material variability and complexity (transverse isotropy, undrained and drained properties), approximately 50 triaxial tests were done per site (Table 2). Of the conducted tests, about 10% experienced technical issues related to equipment malfunctioning or anomalous specimen response (e.g. unrealistic stress path evolution, low strength). Those results are discarded from the analysis in this paper. As a quality assurance measure, at least two of the three subcontracted laboratories were testing core material from the same borehole.

3. Test results

This section presents the results of the experimental campaign, which are reported referring to the effective mean stress (p') and the deviatoric stress (q), or axial (σ'_a) and radial effective stress (σ'_r),

where:

$$p' = \frac{\sigma'_a + 2\sigma'_r}{3} \tag{1}$$

$$q = \sigma'_a - \sigma'_r \tag{2}$$

The maximum value of q during shearing is denoted as q_{Max}. The stress level at which the maximum pore pressure, U_{wMax}, occurred is noted on the stress paths, together with the maximum AB value (AB_{Max})[23], where AB is the ratio between ΔU_w and Δq.

3.1. Basic properties

The bulk density and water content (Table 1) were measured on each tested specimen. On several tested specimens or spare materials from the same sections, mineralogical analyses were also conducted. The information allows for assigning geotechnical properties and composition to each mechanically tested specimen.

For each specimen, in Fig. 2a, the mineralogical clay content is reported versus the bulk density. The water content (at the beginning of the test) is reported versus the corresponding bulk density in Fig. 2b. The plots show that for higher clay content the material has generally lower bulk density and that the lower the bulk density, the higher the water content. These results are in line with previous observations in Opalinus Clay shale[4,11,17], which shows that the lower bulk density can be attributed to both a lower solid density and a higher porosity of the specimens with higher clay content.

3.2. Specimen saturation

Specimen saturation was verified by performing Skempton's B tests: isotropic stress increments are applied in undrained conditions, and the generated pore pressure increment is measured. Generally, two to three increments were performed per specimen, and the pore pressure was left to equilibrate for a minimum duration of 8 h. The pore pressure buildup is sensitive to the system compressibility, including the pore pressure transducers, the tubing, and in particular the volume of water retained by the system. Each laboratory estimated the volume of water in their triaxial apparatuses (dead volume) in undrained conditions. While Lab C system allowed a negligible dead volume, the volumes for labs A and B were respectively 2´200 mm^3 and 700 mm^3. Several authors showed that water volume and compressibility, as well as the specimen solid and bulk compressibility, play a major role in the B measurement (e.g., [3,9,27]) and proposed a correction formula to account for these effects:

$$B_{correct} = \frac{1}{\frac{1}{B_{obs}} - \frac{V_L}{V}\frac{K}{K_f\left(1-\frac{K}{K_s}\right)}} \tag{3}$$

Table 2
Overview of the performed tests.

Site	JO		NL			ZNO	
Borehole	BOZ1-1	BOZ2-1	STA2-1	STA3-1	BUL1-1	MAR1-1	TRU1-1
Undrained tests	19	18	10	10	28	16	26
Drained tests	2		2	3	3	3	3
Total per bh	21	18	12	13	31	20	29
Total per site	39		56			49	
P-specimens	14		35			20	
S-specimens	22		16			19	
Z-specimens	3		5			10	

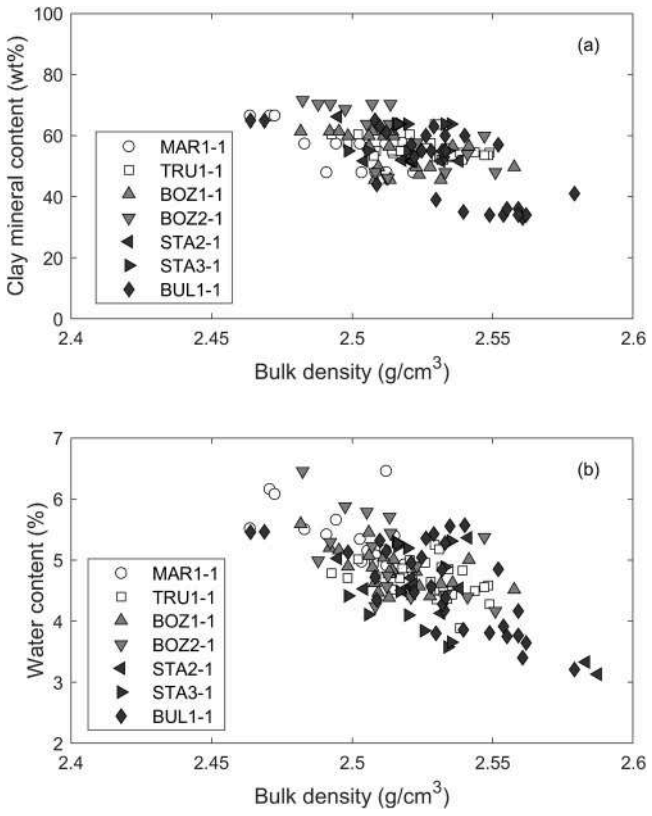

Fig. 2. Clay mineral content (a) and initial water content (b) versus bulk density of the specimens.

The formulation uses B_{obs}, the measured B value, V_L, the volume of fluid in the porewater lines, V, the volume of the specimen, K, the bulk modulus of the specimen, K_f, the bulk modulus of the pore fluid and K_s, the bulk modulus of the solid phase. For the purpose of this calculation, bulk, fluid, and solid moduli are assumed to be $K = 5$ GPa, $K_f = 2.2$ GPa, and $K_s = 50$ GPa, respectively. In Fig. 3 the results of B values for tests from borehole TRU1–1 are reported as an example. It is observed that the applied correction reduces the discrepancies among the laboratories' measurements and the overall variability of the values.

A small stress dependency of the B value on the effective confinement is found within the observed stress range.

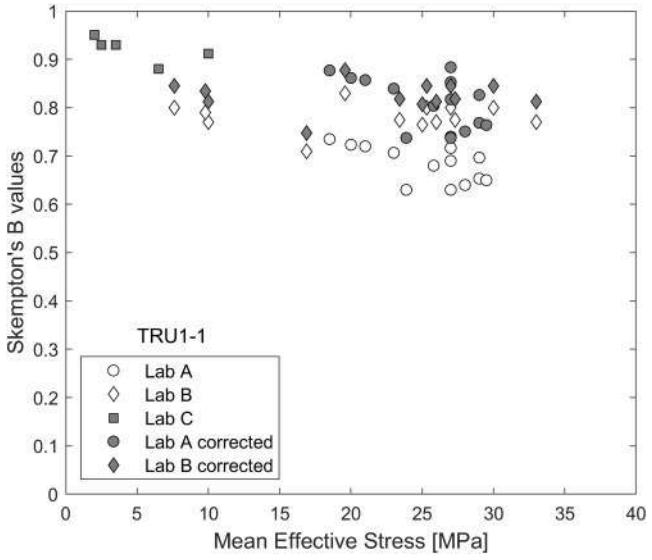

Fig. 3. Skempton's B coefficient measured by the laboratories and corrected accounting for the volume of water in the triaxial systems. Data from borehole TRU1–1 (redrawn after [6]).

3.3. Shearing phase

3.3.1. Strain rate, temperature, and brine composition effects

The main testing program was performed following the testing procedures described in Section 2.3. Throughout the main campaign, variations to the procedure were adopted in a small number of tests to explore their potential impact on test results. The variation from the described procedure addressed the effect of strain rate, temperature, and composition of the synthetic pore fluid. An overview of this comparison is presented in this section, with emphasis on the stress path evolution during the shearing phase.

3.3.1.1. Strain rate assessment. The theoretically admissible strain rate for balanced pore fluid pressure distribution in the specimen can be calculated from the specimen size, drainage configuration, and consolidation coefficient. Drained consolidation phases were performed to bring each specimen to the target stress state for shearing. In the majority of the cases, unloading was performed, since at the end of the saturation state the stress state was higher than the target for shearing. Also, the unloading was performed over a large mean stress difference, in the order of 10 to 20 MPa. Since the unloading is non-instantaneous, constraining consolidation coefficient was not straightforward, and strain rates were defined based on previous recent testing experience with Opalinus Clay[7,10,19]. Strain rates between 1×10^{-7} and 1×10^{-8} 1/s were adopted, depending on the drainage conditions, the specimen sizes, and the presence of lateral and side drains[7].

As an additional quality-control measure, one undrained test was repeated using a five times lower strain rate. Results are shown in Fig. 4 for a set of specimens from the same section in borehole STA3–1: tests A1, A2, A3, and A5 were undrained tests, conducted at a strain rate 1×10^{-7} 1/s. Test A6 is an undrained test conducted at 2×10^{-8} 1/s, which is the same rate adopted for the drained test A4.

The ensemble of the tests shows very high consistency in terms of shear strength evolution with confining effective stress and stress paths, and the three tests at initial p′= 13 MPa show great repeatability. The results support the appropriateness of the adopted strain rates.

3.3.1.2. Pore fluid impact. A second set of specimens were tested to

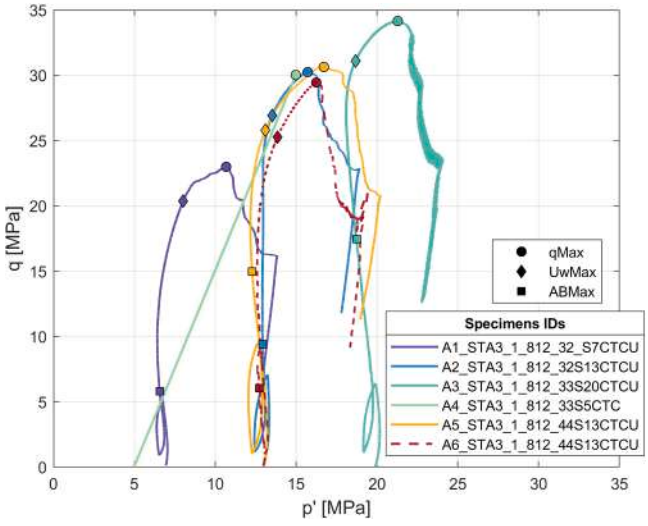

Fig. 4. Test results (S orientation) from a section in borehole STA3–1, depth of 812.4 m. Shearing of test A6 was conducted at a strain rate 5 times slower than the other undrained tests from the same section.

investigate the effect of water composition on the shearing response. Tests B1 to B5 in Fig. 5 were conducted with a brine that mimics the in-situ pore water composition. Test B7 was conducted on a specimen from the same core section as the previous tests, but using distilled water in the pore lines. While an impact of the different pore water fluid chemistry could be expected [24,28], no significant effect is observed in the performed tests. It is furthermore highlighted that the shearing phase of test B5 was conducted in drained conditions, while the shearing phases in tests B1, B3, B4 and B7 were conducted in undrained conditions. In this case as well, the ensemble of the tests shows high consistency.

3.3.1.3. Temperature. The in-situ temperature at the investigated depth is about 35 to 50 °C, hence approximately 10 to 30 degrees higher than standard laboratory testing conditions. The potential impact of the difference between laboratory and in situ temperature on the mechanical properties was investigated with dedicated tests.

Two pairs of tests were performed on the same section of the borehole: for the first pair, specimens were sheared at room temperature. For the second pair, specimens were heated in drained conditions after the consolidation phase and then sheared at a constant temperature (60 °C). The heating was performed in two steps (15 – 20 °C each), with a heating rate of 1 °C/h to limit the temperature-induced pore pressure build-up. At the end of each phase, the temperature was halted for a few hours to assess the evolution of the pore pressure and the strains and allow for potential overpressure dissipation.

Both samples experienced a small volumetric (<< 1%) expansion during heating. The stress paths of the high and low-temperature tests show comparable evolutions (Fig. 6). No relevant impact of temperature on stiffness or strength was found. Accordingly, the remaining testing program was performed at room temperature.

3.3.2. Peak and post-peak shear strength

During shearing the specimens reach a maximum deviatoric shear stress (hereafter peak shear strength), then a quasi-brittle response is observed leading to a decline in the sustained shear stress. In Fig. 7, the peak axial stress of all the tested specimens is reported, and marker colors highlight the loading direction with respect to bedding planes. Results are reported in terms of axial versus radial effective stress. It is noted that the Z-specimens yielded the lowermost strength, across the entire range of tested confinements. S and P-specimens showed a similar response, and the results partially overlap, but the P-specimens show a tendency for higher strength across the tested confining range, yet differences fade towards the lower end of the confinement range.

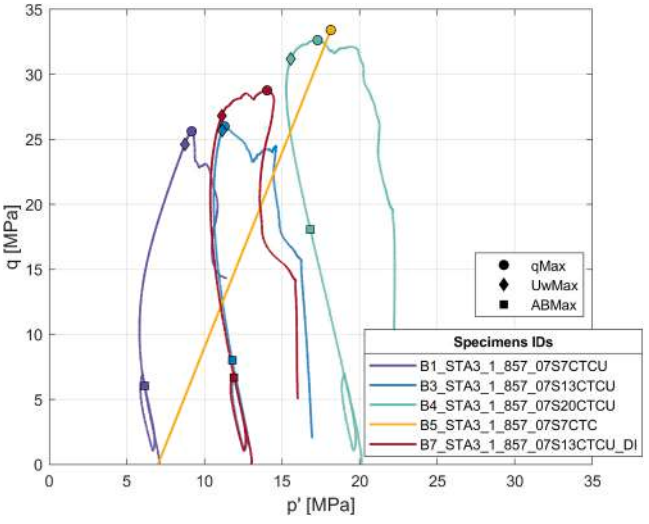

Fig. 5. Test results (S orientation) from a section in borehole STA3–1, depth of 857.1 m. Test B7 was conducted with distilled water instead of brine.

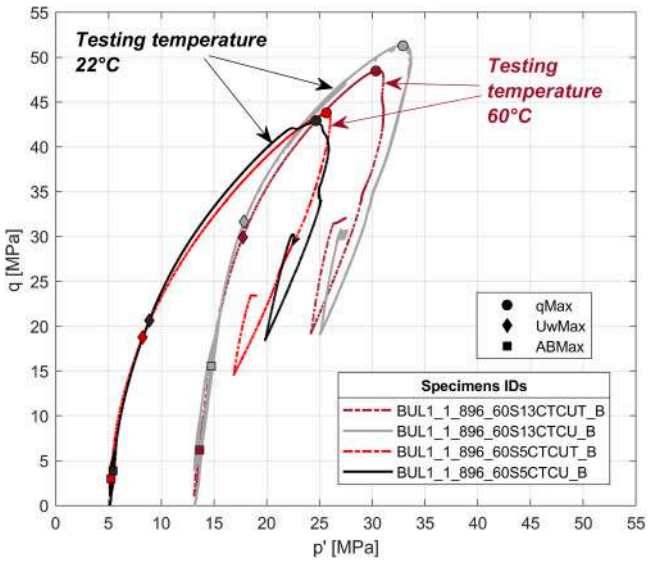

Fig. 6. Stress paths for S-specimens sheared at ambient (room) and high (60 °C) temperature. Specimens are from a section in borehole BUL1-1, depth of 896.6 m.

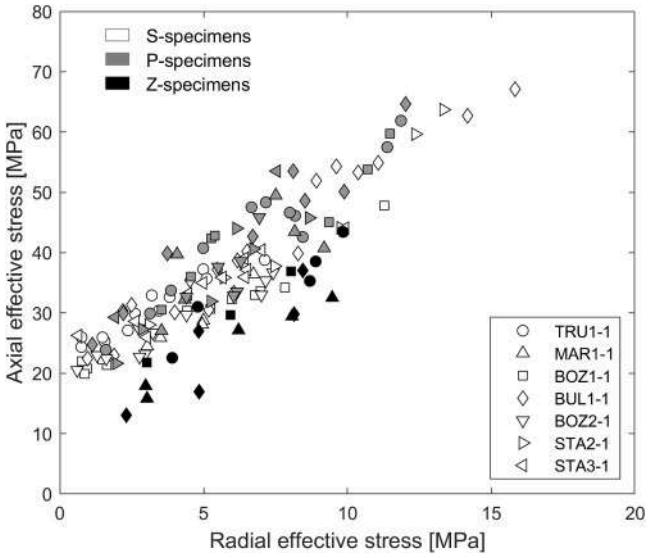

Fig. 7. Axial versus radial effective stress at peak for S, P, and Z-specimens.

It is further noted that two Z-specimens in BUL1–1 showed a particularly low peak shear stress, while their post-peak strength results are in line with the other results (Fig. 8). The low peak strength may be related to pre-existing fissures formed during specimen coring. Specimens coring at an angle to bedding proved generally more challenging, and potential bedding-parallel micro-fissures have greater relevance in this orientation as the shearing plane forms in the direction subparallel to the bedding planes.

Data related to the post-peak condition were processed taking into account that, as a consequence of the failure (identified as the maximum deviatoric stress), the specimen was divided into two blocks which slid one over the other along the inclined shear band. Post-peak strength was analyzed for the strength achieved after the peak, once the deviatoric stress stabilizes. The stress state on the formed failure surface was evaluated.

In the framework of a sliding block analysis, the evolution of the contact surface with the axial displacement was considered. In the limited strain range needed to reach constant deviatoric stress after the

peak, the effect of the contact surface change was found to be limited, and therefore neglected.

For each specimen, the inclination of the shear band was evaluated from the pictures of the specimen after the test. Results showed a different average inclination among the loading orientations:

- S-specimens shear band inclination with respect to the horizontal plane: 57 ± 7° (median ± standard deviation)
- P-specimens: 68 ± 5°
- Z-specimens: 61 ± 5°, which approximately corresponds with the inclination of the bedding direction of the specimen, i.e. the shearing developed along the bedding direction.

The shear (τ) and normal effective stress (σ'_n) on the failure surface were derived once q stabilizes after peak, from the stress state (axial and radial effective stress) projected onto the failure surface plane of known inclination. The results are plotted in Fig. 8.

3.3.3. Elastic properties

The elastic transversely isotropic undrained moduli E_u and Poisson's ratios here reported were calculated over the unloading path before the peak. Considering its non-linearity, in each test the elastic modulus is computed as the tangent modulus during unloading for a fixed strain range, ε_a= 0.02%– 0.04% [5], measuring the strain from the beginning of the unloading phase.

Results for S-specimens (moduli perpendicular to bedding) and P-specimens (moduli parallel to bedding) are reported in Fig. 9. It is noted that both S and P-specimen results showed a dispersion in the E_u values.

The two Poisson's ratios in undrained conditions were estimated: from S-specimens, the ratios of the radial (parallel to bedding) to axial (perpendicular to bedding) strains, $\nu_{u\perp}$, were in the range 0.3–0.6; from P-specimens, the ratios of the radial (parallel to bedding) to axial (parallel to bedding) strains, $\nu_{u\parallel}$, were in the range 0.2–0.35.

4. Discussion

4.1. Representativeness

From complementary laboratory analysis (mineralogical, hydrogeological and geochemical campaign), a high number of cores were evaluated at a regular spacing of approximately 2 to 5 m depth[15]. In all these cores, bulk mineralogy, water content, and bulk density were

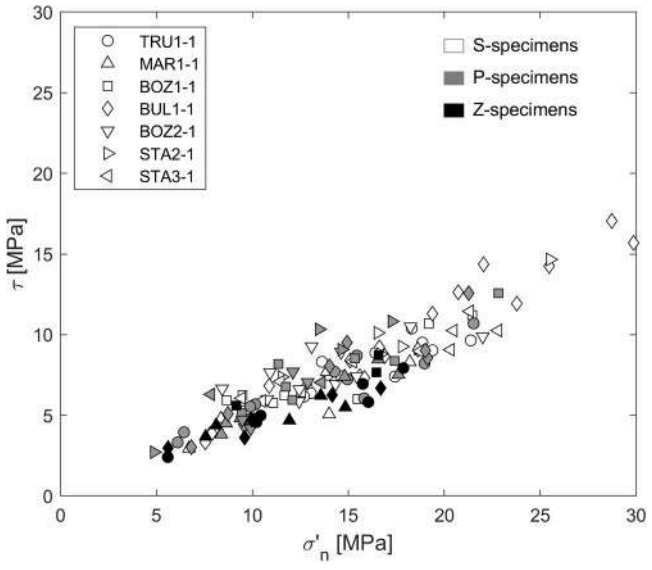

Fig. 8. Shear and normal effective stress acting on the failure surface at post-peak for P, S, and Z-specimens.

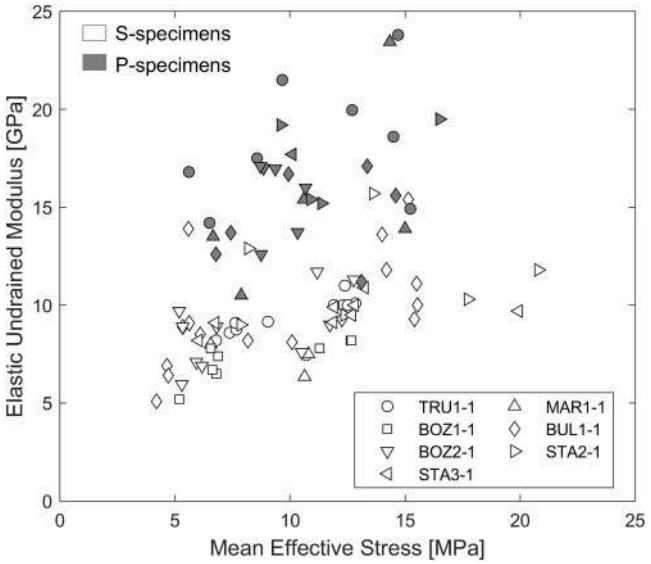

Fig. 9. Elastic undrained moduli for S and P-specimens.

constrained with the same techniques. In addition, geophysical logs were calibrated to core data (referred to as MultiMin[2]) to provide a continuous, semi-empirical estimate of basic properties and bulk mineralogy with depth (one data point every 15 cm). These results provide a detailed characterization of the Opalinus Clay over the entire formation thickness, showing the variability in the mineralogical composition and physical properties of the formation.

Specimens from the geomechanical campaign were sampled from several depths in each borehole, to account for potential heterogeneities. The depth of the tested specimens and the corresponding bulk densities are reported in Fig. 10, together with those of the complementary laboratory campaign[15], for all boreholes. It is shown in Fig. 10 that the wide range of depths investigated in the geomechanical campaign covers approximately the same range as the complementary laboratory

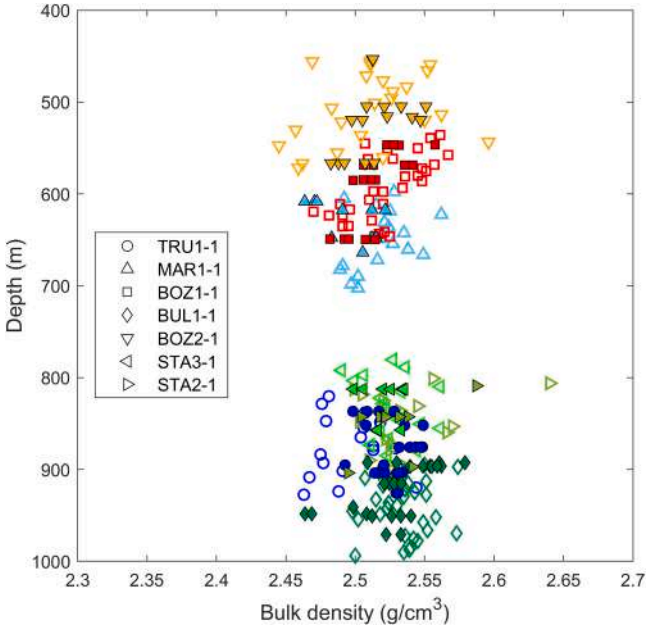

Fig. 10. Variability in the bulk density from complementary laboratory campaign ([15], open symbols), and the geomechanically tested specimens (this study, filled symbols). Results are plotted versus the sourcing depth of the specimen in each borehole.

campaign per each borehole, i.e., the entire formation thickness.

The frequency of occurrence of the geomechanically tested specimen versus their clay mineral content is reported in Fig. 11, together with the laboratory results of complementary testing programs (about 300 measurements[15]) and the MultiMin distributions (600-800 points per borehole[2]).

The comparison of the three sets of results supports the conclusion that the geomechanical tests are very much representative of the entire spectrum of compositional variability in the formation. However, the low clay content specimens (<40%) appear to be slightly over-represented in the triaxial tests, with respect to the actual occurrence within the formation. It was moreover observed in the petrophysical distributions, that low clay content sections rarely occurred for a length longer than a few tens of centimeters, therefore their impact on the overall formation response is considered marginal.

4.2. Differences among sites and depths

In this testing campaign, Opalinus Clay was investigated in 7 boreholes among three sites, where the formation depth varies between 450 and 1000 m. The potential effect of the different current burial can be verified, by comparing results from the shallower locations (boreholes BOZ1–1, BOZ2–1, MAR1–1) and the deeper locations (boreholes BUL1–1, TRU1–1, STA2–1, STA3–1).

The peak shear strength is reported in Fig. 12, by borehole (markers) and bulk density (color bar).

It is noted that for loading in the direction perpendicular to bedding (S-specimens), the specimens from the shallower locations (BOZ1–1, BOZ2–1, MAR1–1) tend to plot in the lower part of the observed range, yet they overlap with results from the deeper locations.

Also, no depth-dependency is observed in the specimens loaded parallel to bedding (P-specimens) or with an angle to bedding (Z-specimens). It is concluded that the effect of the current depth in the observed range across all sites has limited effects on the geomechanical parameters, i.e. it is comparable with the overall variability of the material properties. Similarly, no clear differences emerge from grouping the results of basic properties and clay mineral content by site (cf. Table 1).

These observations are in line with the common geological history to which the formation was subjected at the regional scale.

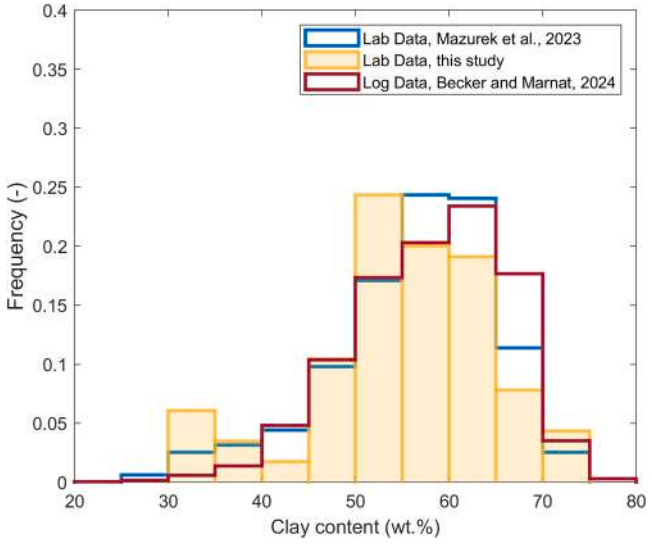

Fig. 11. Frequency of the clay mineral content in the geomechanically tested specimens (this study) and frequencies from the other testing campaigns.

4.3. Effect of the mineralogical composition on the mechanical parameters

The peak and post-peak shear strengths are separately interpreted by adopting the Mohr-Coulomb failure criterion:

$$\sigma_a'(1 - \sin\varphi') = \sigma_r'(1 + \sin\varphi') + 2c'\cos\varphi' \quad (4)$$

Where the c' is the effective intercept cohesion and φ' is the mobilized shear strength angle.

The strength results were grouped by tested specimen loading orientation with respect to bedding. Then, for each geometry, results were further split by borehole, bulk density (4 intervals), and mineralogical composition (4 intervals). For each of those groups, linear regressions were derived. The two Z-specimens showing low strength (cfr. Section 3.3.2) were not used for the regressions. The median of the derived parameters, as well as those yielding the minimum and the maximum regression line are reported in Fig. 12. For the S direction, results from the higher bulk density specimens (i.e. lower clay content) tended to exhibit higher peak strength, compared to low bulk density (i.e. higher clay content). The differences seem negligible for the P and Z directions.

It is emphasized that the peak strength effective confinement in undrained conditions depends on the pore pressure evolution during the shearing: for the same initial effective confinements, low clay content (and high bulk density) specimens showed higher effective confinement and higher strength, hence they are better represented in the range of radial effective confinement higher than 10 MPa. The opposite occurs for higher clay content specimens, i.e. those results are better represented in the lower confinement range. As a consequence, a single regression line (Fig. 12, *Regression-All*) considering the entire set of results, neglecting composition differences, would lead to an overestimation of the regression line inclination, and an underestimation of the intercept (cf. Section 4.4).

It is noted that, within the observed stress range, the effect of a slightly higher (or lower) inclination on the strength estimate is limited, considering the high number of tested specimens, and the small heterogeneity in the material response within the observed stress range.

As a general remark, it is emphasized that, if only a few test results are available, ignoring the heterogeneity among specimens may lead to a misinterpretation of the material parameters, more so if extrapolating outside of the stress range of observation.

For the post-peak strength, median regression, and upper and lower bounds are defined in the τ-σ'_n plane (Fig. 13). Also for the post-peak strength, the specimens with higher bulk density (i.e., lower clay content) showed higher post-peak strength, achieved at higher confinement. The opposite is observed for low bulk density specimens (i.e., higher clay content). The reported lower bound corresponds to the one adopted for the shaly facies of Opalinus Clay from the Mont Terri Rock Laboratory by ref. [19].

In the current testing campaign, a detailed analysis of the effective intercept cohesion (c') and mobilized shear strength (φ') evolution with strain was conducted and is reported in Section 4.4.

In the elastic moduli, a dispersion of results in both the S and P direction is observed. Nonetheless, in the S-specimen results, a correlation with the bulk density can be identified: the higher the bulk density, the higher the stiffness (see also Section 4.5, Fig. 16). High bulk densities are observed in specimens with low clay content, as shown in Section 3.1. Those results belong to the top of the Opalinus Clay formation in BUL1–1 and STA2–1.

4.4. Post-peak analysis

After the peak is reached, the deviatoric stress progressively reduces with increasing strains, up to reaching a stable value. In some cases, pore pressure kept evolving during axial strain increases, despite achieving a

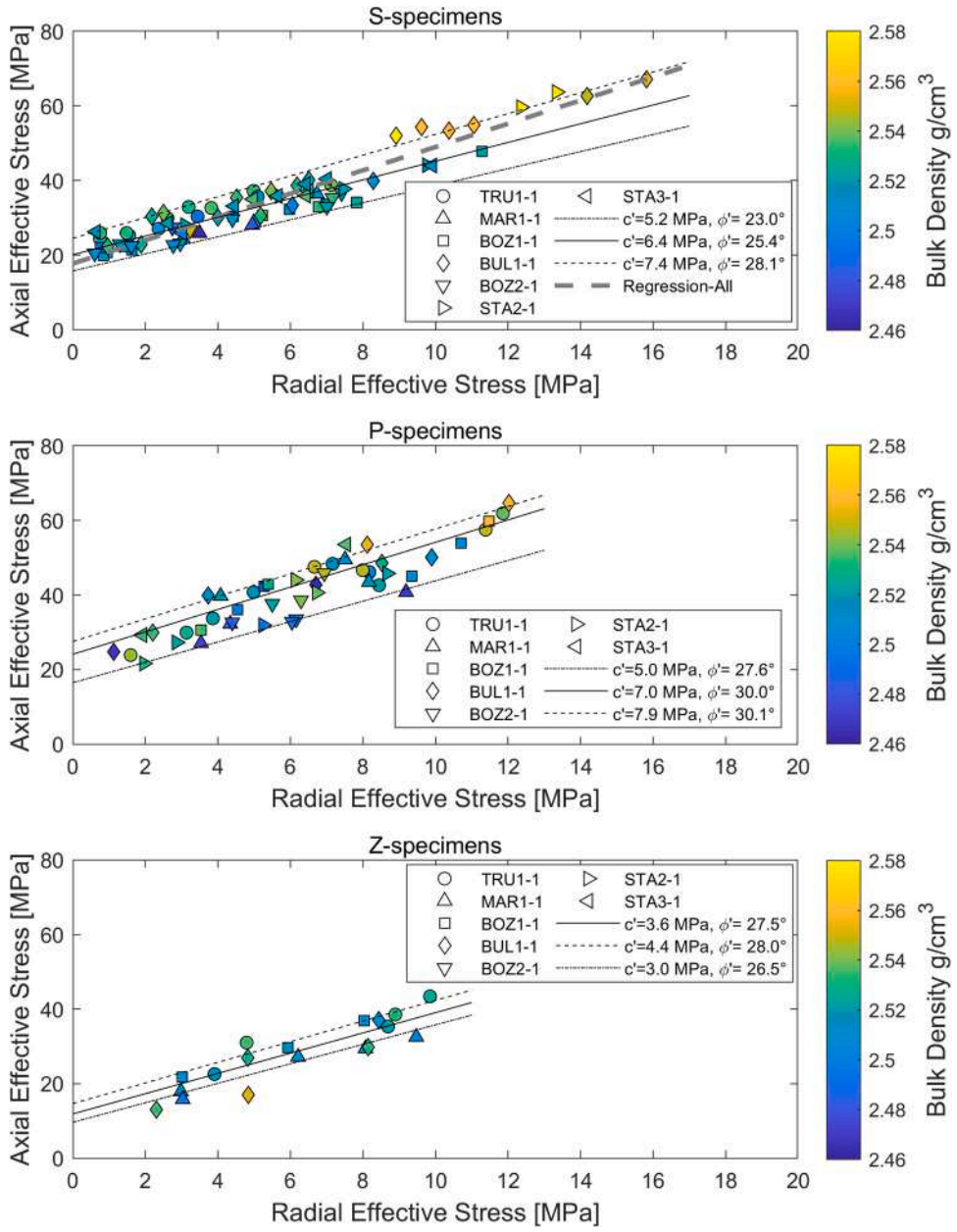

Fig. 12. Peak axial stress of Opalinus Clay specimens with S, P, and Z geometry. Results are sorted by sampling borehole (marker) and bulk density (color bar). The Mohr-Coulomb regression lines for the median, maximum, and minimum values are shown.

rather stable q. This response raises the issue of defining the post-peak strength of the specimen. Further analysis was therefore conducted.

The stress state evolution was re-interpreted as a function of the axial strain from the peak to the post-peak (Fig. 14). In this analysis, the strains reported in the following figure are measured setting the zero at the peak shear strength, and therefore the axial strain values are reported from that point on, e.g., evaluating the softening response independently from the elastic and hardening response.

The results for undrained S-specimens are reported in Fig. 15. The analysis includes specimens from all boreholes and neglects the density and mineralogy heterogeneity. It is worth noticing that the first curve ε_a= 0 [-] corresponds to the regression across all the S-specimens at the peak shear strength on the inclined shear plane, and a higher shear strength angle and lower cohesion are obtained (as mentioned in Section 4.3).

While the cohesion is mobilized at peak strength, it reduces negative exponentially with strain, as typical for brittle and quasi-brittle materials[13]. On the other hand, the mobilized shear strength reduction is less pronounced.

The last regression line at ε_a= 0.02 (-), would lead to an unrealistic negative intercept, hence the regression is forced through zero as the lowest bound.

4.5. Anisotropic stiffness

The undrained elastic properties were obtained for an effective confining stress range of 4 to 20 MPa, and the results are plotted in Fig. 16. The specimens with a lower bulk density, typical of the clay-mineral richer specimens, yielded moduli (E_u) in the lower part of the range, for the direction perpendicular to bedding. Higher moduli are generally observed at higher confinements. Results for loading direction perpendicular to bedding (S-specimens) were fitted with a power law for the range 4 to 20 MPa effective confinement (Fig. 16a):

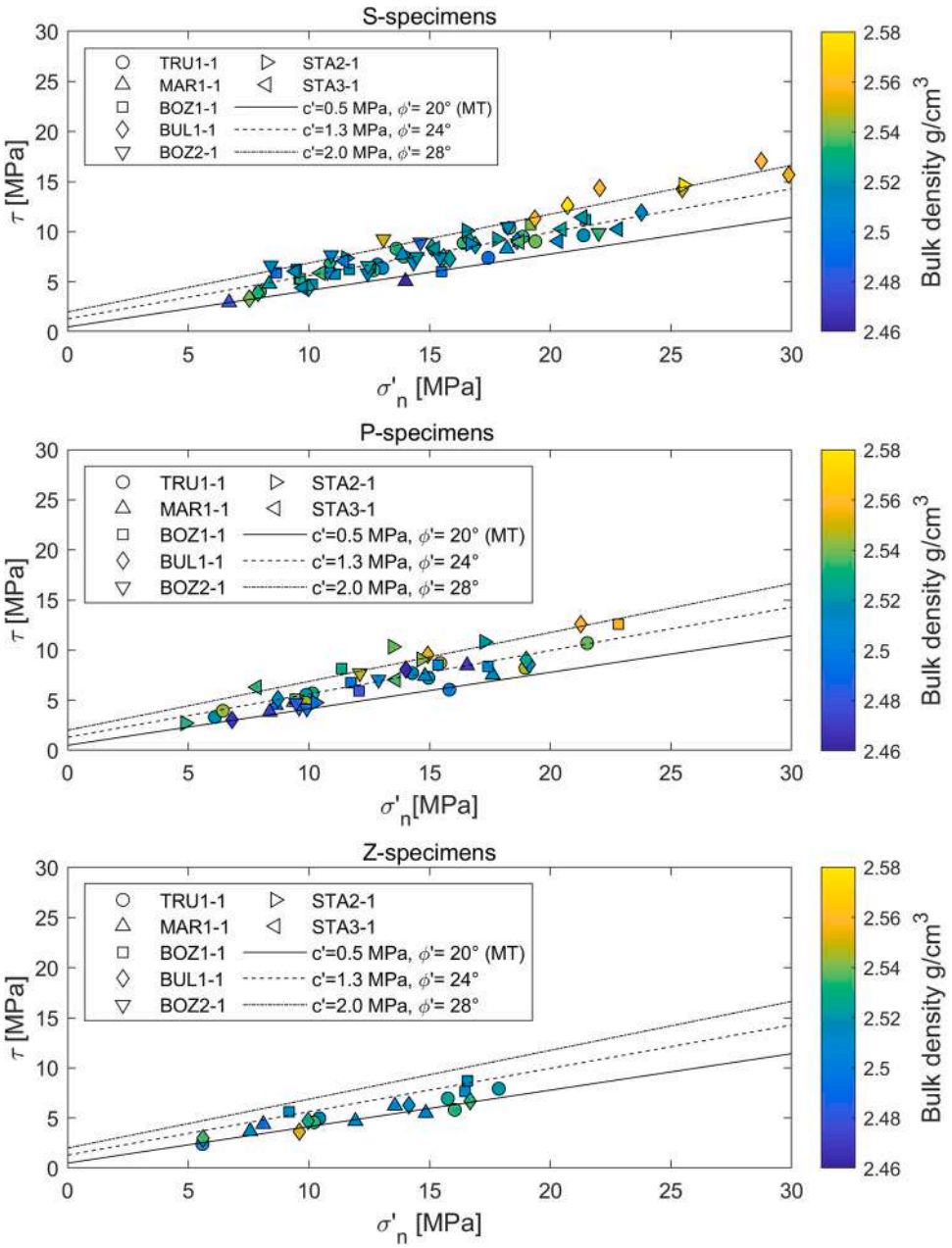

Fig. 13. Post-peak strength, Opalinus Clay specimens with S, P, and Z geometry.

$$E_{u\perp}=4{\cdot}08{\cdot}p'^{0{\cdot}34} \quad (5)$$

Two bounds to moduli dispersion were identified by shifting the above power law of 2 GPa towards higher and lower moduli.

The highest values of the $E_{u\perp}$ moduli (10–15 GPa) were obtained on high-density specimens (> 2.52 g/cm^3) corresponding to low clay content (<40 wt%). As discussed in Section 4.1, the occurrence of low clay content layers appears to be limited, and these Opalinus Clay specimens are overrepresented in the geomechanical testing program, with respect to their extent along the boreholes. For the purpose of defining suitable regression law to represent the evolution of the elastic moduli with the confinement, those high stiffness values are neglected.

Results in the direction parallel to the bedding show a less clear trend with composition or confinement (Fig. 16b). Analysis of comparable laboratory specimens tested in the direction parallel and perpendicular to bedding shows an anisotropic ratio $E_{u\parallel}/E_{u\perp}$ ranging between 1.5 and 2.5, with an average value of 2.0. Power law regression for the direction parallel to bedding was therefore obtained by multiplying by a factor 2 the power law in the direction perpendicular to bedding. Similarly, the minimum and maximum bounds were defined (Fig. 16). The so-created bounds enclose, with few exceptions, the observed data points.

4.6. Comparison with Mont Terri

As most of the existing geomechanical testing data of Opalinus Clay stems from cores sourced at the Mont Terri Rock Laboratory, we compare these data with those obtained from the TBO campaign.

In Fig. 17, the range of peak and post-peak axial stress observed in the deep borehole campaign (S-specimens) are reported (white markers), together with the results obtained from Mont Terri specimens tested adopting similar protocols. Results from the sandy (3–13% porosity, 14–39 wt% clay-mineral content) and shaly (12–17% porosity, 58–71 wt% clay-mineral content) lithofacies are shown[5,8,19].

The range of results in the deep borehole shows consistently higher peak axial stress than the results from Mont Terri. Specimens from the sandy facies of Mont Terri show peak strengths in a similar range as from

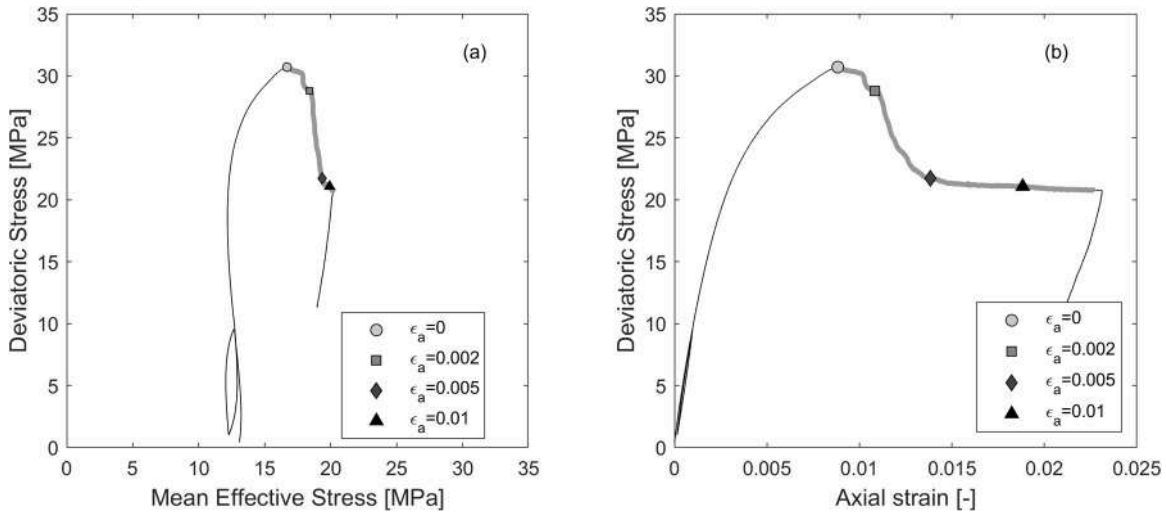

Fig. 14. Stress path (a) and stress-strain curve (b) picked (markers) in the softening part of the curve.

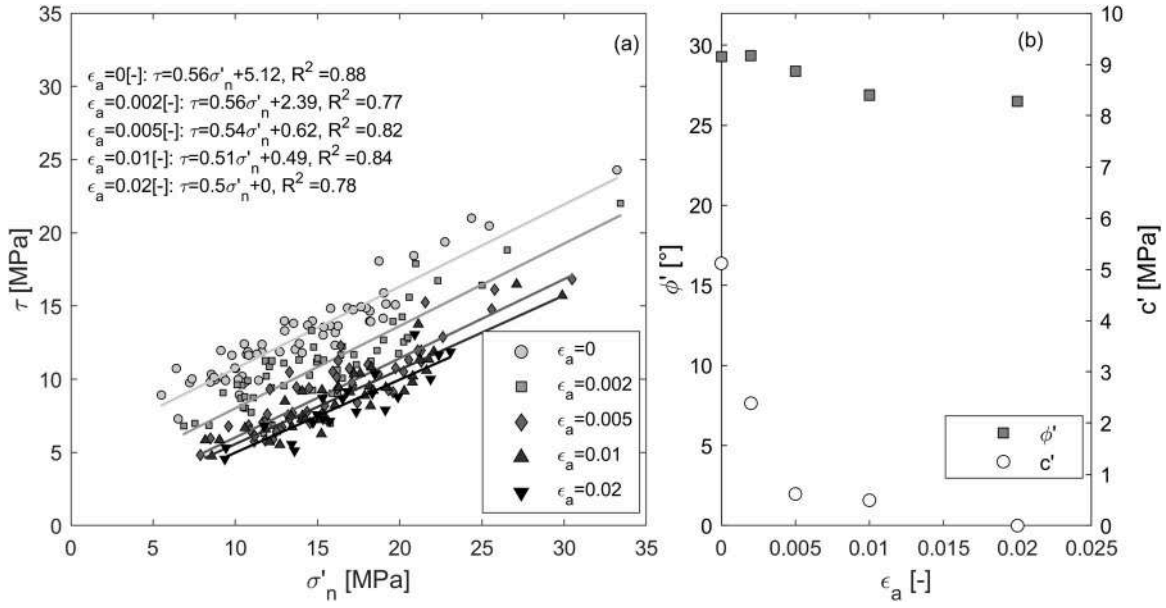

Fig. 15. Shear stress versus normal effective stress evolution with axial strain, moving from the peak shear stress up to 2% strain. Mohr-Coulomb regressions (a) and mobilized shear strength angle and effective intercept cohesion of the regressions (b).

cores of the deep boreholes, yet with larger dispersion, which had been associated with the mineralogical composition of the specimens[5].

Compared to the clay-mineral rich facies in Mont Terri (shaly facies), the results from the deep boreholes show, for a similar composition, a substantial reduction in porosity, from 12–17% at Mont Terri to 10–13% at greater depth in the siting regions, and an increment in the peak strength. This also leads to lower variability in strength across different mineralogies in Opalinus Clay at the siting regions.

In terms of Mohr-Coulomb regression parameters, the results from the deep borehole show an effective cohesion twice as high as the Mont Terri data, while shear strength angles are within a similar range. Overall, the material from the deep borehole shows a significantly enhanced peak strength, with calculated UCS values 2–3 times higher than in Mont Terri.

On the other hand, the post-peak properties of the results from the deep boreholes, are rather in line with the results from previous testing campaign on Mont Terri specimens. Both in terms of effective cohesion and shear strength angles derived for the post-peak condition, the results of Mont Terri fall into the same range obtained from the deep borehole testing campaign.

The formation at the Mont Terri URL, currently at depth of 220–320 m below ground, has experienced a maximum estimated burial depth of 1350 m[14], therefore both maximum and current burial depth are higher in the siting region.

It could be inferred that in the siting regions, the stress history has had a predominant effect on the material peak shear strength: the higher stresses and temperature have acted on the diagenesis of the material, reducing the porosity and increasing the particles interlocking and bonding, while the relevance of the minerals composing the material has been, in comparison, reduced. Conversely, once the cohesion has been degraded, as in the post-peak condition, the material response is dominated by the friction along the failure surface which is tied to the mineralogical composition of the material. In this respect, the Mont Terri and TBO results are comparable.

For what concerns the elastic properties, Mont Terri results (e.g., [5,19]) in the direction perpendicular to bedding exhibit undrained elastic

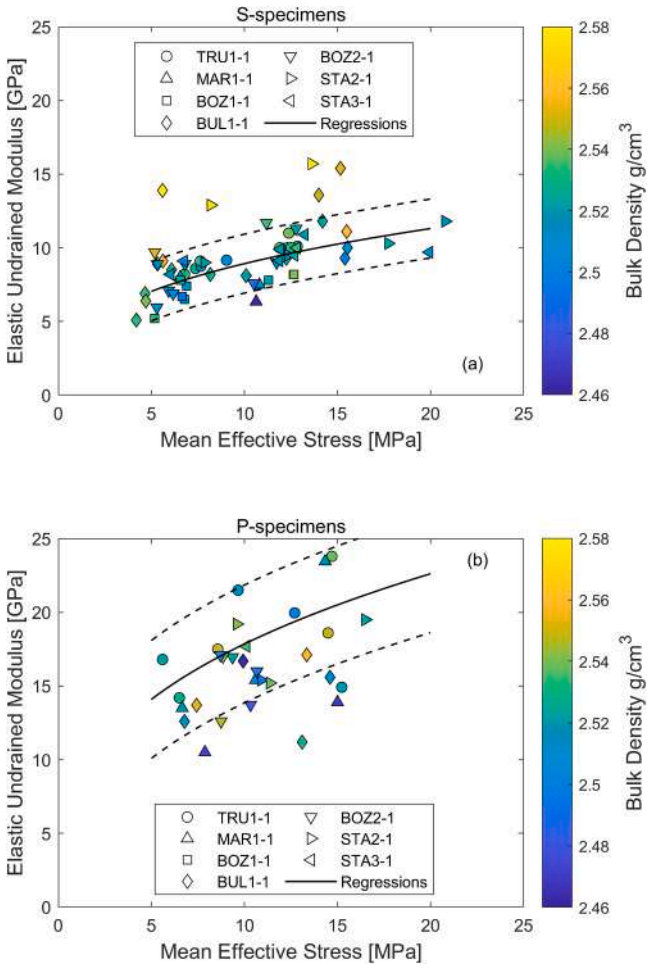

Fig. 16. Elastic undrained moduli of P and S-specimens sorted by specimen initial bulk density, including potential regression lines.

moduli of 2.5 to 7 GPa, with a maximum value of 9 GPa, for carbonate facies at the maximum effective mean stress of 15 MPa. Tests results parallel to bedding showed values between 7.8 and 10.7 GPa. Table 3 summarizes the comparison between MT and TBO elastic properties.

It is remarked that, as for shear strength, the undrained elastic modulus is higher in the deep borehole results, both in the direction perpendicular and parallel to the bedding. The first is 60%– 120% higher, while the latter is 30% to 200% higher. The variability in the increment in parallel to bedding direction reflects the dispersion of the data, already observed in Section 3.3.3.

The two Poisson's ratios in undrained conditions (cf. Section 3.3.3) are also compared in Table 3. These results present generally a large dispersion, yet the results span over similar ranges.

5. Conclusions

An extensive laboratory testing program with core material of Opalinus Clay shale from seven deep boreholes and three site regions was carried out to constrain the hydromechanical properties of Opalinus Clay for the design and safety assessment of a future repository and identify possible site-specific differences in geomechanical properties. Dedicated procedures of core conditioning, specimen selection, specimen preparation and test execution were adopted and systematically implemented for more than 140 experimental tests. Additional tests were conducted to confirm the adequacy of the used deformation rate, the chemistry of the pore fluid and the chosen temperature to perform the tests.

Based on the comparison of bulk density, water content and clay mineral content, the tested specimens can be considered as representative for the variability of the formation at the scale of tens of centimeters to tens of meters.

The exceptionally high number of triaxial tests on one shale formation allows for a detailed analysis of the variability of the material properties of Opalinus Clay. The following main conclusions can be drawn:

- The relatively large variation in mineralogy (clay-mineral content varying between approximately 30 to 75 wt%), is not manifested in a large variation of strength. The calculated UCS from the triaxial test

Table 3
Summary elastic undrained moduli and Poisson's ratios from Mont Terri (MT) ([a] in ref [5]; [b] in ref [19]) and TBO campaigns. [c] Range for parallel to bedding refers to the strategy presented in Section 4.5. For the full range of values the reader is referred to Fig. 9.

	Loading direction (to bedding)	E_u (GPa)	ν_u (-)	p′ (MPa)
MT	⊥	2.5 – 7[a,b]	0.2-0.5[b]	4–16[a,b]
	∥	7.8 – 10.7[b]	0.1-0.55[b]	4–10[b]
TBO	⊥	5-12	0.3-0.6	5-15
	∥	10-24[c]	0.2-0.35	5-15

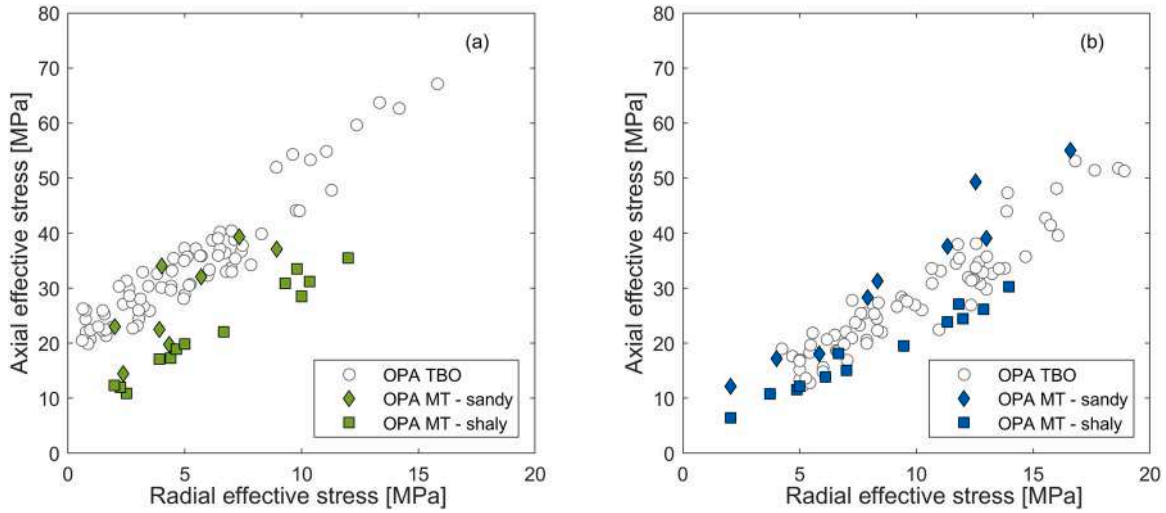

Fig. 17. Peak (a) and post-peak (b) axial versus radial effective stress of S-specimens, from Mont Terri sandy and shaly facies [5,19] and TBO data.

results for the direction perpendicular and parallel to bedding is of the order of 21 ± 5 MPa, i.e. it exhibits only very moderate variation. Nonetheless, a tendency to higher strength with lower clay content (generally higher bulk density) is identified.

- In the explored in-situ depth range between 450 to 1000 m below ground among the three studied sites, a negligible correlation of material properties with depth and site of recovery is observed, consistent with limited differences in the compaction state and porosity.
- Assuming a Mohr-Coulomb failure criterion interpretation, the transition from peak to post-peak comes at the expense of cohesion, i.e., a reduction of cohesion close to zero with only a minor reduction of the mobilized shear strength angle.
- A dependency on the specimens' composition and density is also observed in the undrained stiffness values, for the direction perpendicular to bedding. A large scatter is however observed for the direction parallel to bedding, where no trend with bulk density can be seen.
- In contrast to the depth range in the siting regions, the shallower burial depth (220 to 320 m) at Mont Terri and the differences in the tectonic and burial history led to significantly different strength and stiffness properties. Both strength and stiffness values for Opalinus Clay are higher in the siting regions than at Mont Terri. Yet the stiffness anisotropy factor of approximately two is consistent with other studies on Opalinus Clay. The results suggest that the different burial history, to which the material in the siting regions was subjected, had impacted the diagenesis of the material, decreasing the porosity and possibly increasing the cementation. This effect seems to vanish towards larger shear strains, once the cohesion is reduced to close to zero, where the results of the TBO fall in the same range as the results obtained in shallower locations.

CRediT authorship contribution statement

Eleonora Crisci: Conceptualization, Methodology, Formal analysis, Writing – original draft. **Silvio B. Giger**: Funding acquisition, Resources, Project administration, Methodology, Conceptualization, Writing – review & editing. **Lyesse Laloui**: Validation, Supervision. **Alessio Ferrari**: Methodology, Supervision, Validation, Writing – review & editing. **Russ Ewy**: Methodology, Supervision, Investigation, Validation, Writing – review & editing. **Rudy Stankovic**: Investigation. **Jørn Stenebråten**: Investigation. **Kristine Halvorsen**: Investigation. **Magnus Soldal**: Investigation.

Declaration of Competing Interest

The authors declare that they have no known competing financial interests or personal relationships that could have appeared to influence the work reported in this paper.

Data availability

Data will be made available on request.

Acknowledgments

Martin Mazurek (RWI, University of Bern, Switzerland) is acknowledged for providing data on mineralogy and grain density, Lukas Keller (ZHAW, University of Applied Sciences Winterthur, Switzerland) for core XCT scanning and processing and Bahman Bohloli (NGI, Oslo, Norway) for the coordination of the investigations at NGI. This study was funded by the National Cooperative for the Disposal of Radioactive Waste (Nagra), Switzerland.

References

1. Amann F, Wild KM, Loew S, Yong S, Thoeny R, Frank E. Geomechanical behaviour of Opalinus Clay at multiple scales: results from Mont Terri rock laboratory (Switzerland). *Swiss J Geosci*. 2017;110:151–171. https://doi.org/10.1007/s00015-016-0245-0.
2. Becker J. Marnat S.Petrophysical data and core calibrated multimineral interpretation. 2024 (Nagra Arbeitsbericht NAB 24-17).
3. Bishop AW. The influence of system compressibility on the observed pore-pressure response to an undrained change in stress in saturated rock. *Géotechnique*. 1976;26:371–375. https://doi.org/10.1680/geot.1976.26.2.371.
4. Crisci E, Ferrari A, Giger SB, Laloui L. Hydro-mechanical behaviour of shallow Opalinus Clay shale. *Eng Geol*. 2019;251:214–227. https://doi.org/10.1016/j.enggeo.2019.01.016.
5. Crisci E, Ferrari A, Giger SB, Laloui L. Effect of the mineralogical composition on the elastoplastic hydromechanical response of Opalinus Clay shale. *Int J Rock Mech Min Sci*. 2021;143, 104747. https://doi.org/10.1016/j.ijrmms.2021.104747.
6. Crisci, E., Giger, S., Laloui, L., 2023, TBO Trüllikon-1–1: Data Report. Dossier IX Rock-mechanical and Geomechanical Laboratory Testing (Nagra Arbeitsbericht NAB 20–09 Rev. 1).
7. Ewy RT. Practical approaches for addressing shale testing challenges associated with permeability, capillarity and brine interactions. *Geomech Energy Environ, Theme Issue Sel Pap Int Workshop Adv Lab Test Model Soils Shales*. 2018;14:3–15. https://doi.org/10.1016/j.gete.2018.01.001.
8. Favero V, Ferrari A, Laloui L. Anisotropic Behaviour of Opalinus Clay Through Consolidated and Drained Triaxial Testing in Saturated Conditions. *Rock Mech Rock Eng*. 2018;51:1305–1319. https://doi.org/10.1007/s00603-017-1398-5.
9. Ghabezloo S, Sulem J. Effect of the volume of the drainage system on the measurement of undrained thermo-poro-elastic parameters. *Int J Rock Mech Min Sci*. 2010;47:60–68. https://doi.org/10.1016/j.ijrmms.2009.03.001.
10. Giger SB, Ewy RT, Favero V, Stankovic R, Keller LM. Consolidated-undrained triaxial testing of Opalinus Clay: Results and method validation. *Geomech Energy Environ, Theme Issue Sel Pap Int Workshop Adv Lab Test Model Soils Shales*. 2018;14:16–28. https://doi.org/10.1016/j.gete.2018.01.003.
11. Houben ME, Desbois G, Urai JL. A comparative study of representative 2D microstructures in Shaly and Sandy facies of Opalinus Clay (Mont Terri, Switzerland) inferred form BIB-SEM and MIP methods. *Mar Pet Geol*. 2014;49:143–161. https://doi.org/10.1016/j.marpetgeo.2013.10.009.
12. Keller LM, Giger SB. Petrophysical Properties of Opalinus Clay Drill Cores Determined from Med-XCT Images. *Geotech Geol Eng*. 2019. https://doi.org/10.1007/s10706-019-00815-2.
13. Martin CD, Chandler NA. The progressive fracture of Lac du Bonnet granite. *Int J Rock Mech Min Sci Geomech Abstr*. 1994;31:643–659. https://doi.org/10.1016/0148-9062(94)90005-1.
14. Mazurek M, Hurford AJ, Leu W. Unravelling the multi-stage burial history of the Swiss Molasse Basin: integration of apatite fission track, vitrinite reflectance and biomarker isomerisation analysis. *Basin Res*. 2006;18:27–50. https://doi.org/10.1111/j.13652117.2006.00286.x.
15. Mazurek M, Gimmi T, Zwahlen C, Aschwanden L, Gaucher E, Kiczka M, Rufer D, Wersin P, Marques Fernandes M, Glaus M, Van Loon L, Traber D, Schnellmann M, Vietor T. Swiss deep drilling campaign 2019–2022: Geological overview and rock properties with focus on porosity and pore-space architecture. *Applied Geochemistry*. 2023. https://doi.org/10.1016/j.apgeochem.2023.105839.
16. Mazurek M., Aschwanden L. Multi-site petrographic and structural characterisation of the Opalinus Clay. 2020. (Nagra Arbeitsbericht NAB19–44).
17. Mazurek, M., Wersin, P., Hadi, J., Opalinus Clay in the shallow decompaction zone: Geochemical investigations on drill core samples from borehole Lausen KB. 2017. (Nagra Arbeitsbericht NAB 16-58).
18. Minardi A, Giger SB, Ewy RT, Stankovic R, Stenebråten J, Soldal M, Rosone M, Ferrari A, Laloui L. Benchmark study of undrained triaxial testing of Opalinus Clay shale: Results and implications for robust testing. *Geomechanics for Energy and the Environment*. 2021;25. https://doi.org/10.1016/j.gete.2020.100210.
19. Minardi A., Ferrari A., Laloui L. Benchmark study on triaxial testing of Opalinus Clay: analysis and comparative evaluation of tests results. 2019. (Nagra Arbeitsbericht NA19–018).
20. Nagra SGT Etappe 2: Vorschlag weiter zu untersuchender geologischer Standortgebiete mit zugehörigen Standortarealen für die Oberflächenanlage: Geologische Grundlagen Dossier II. Sedimentologische und tektonische Verhältnisse. 2014.(Nagra Technischer Bericht 14–02).
21. Nordas AN, Brauchart A, Anthi M, Anagnostou G. Calibration method and material constants of an anisotropic, linearly elastic and perfectly plastic Mohr-Coulomb constitutive model for Opalinus Clay. *Rock Mech Rock Eng*. 2023. https://doi.org/10.1007/s00603-023-03509-7.
22. Rufer, D., Stockhecke, M., 2021, Field manual: Drill core sampling for analytical purposes (No. Nagra Arbeitsbericht NAB 19–13 Rev. 1).
23. Skempton AW. The Pore-Pressure Coefficients A and B. *Géotechnique*. 1954;4:143–147. https://doi.org/10.1680/geot.1954.4.4.143.
24. Tuttolomondo A, Ferrari A, Laloui L. Generalized effective stress concept for saturated active clays. cgj-2020-0390 *Can Geotech J*. 2020. https://doi.org/10.1139/cgj-2020-0390.
25. Wetzel A, Allia V. Der Opalinuston in der Nordschweiz: Lithologie und Ablagerungsdichte. *Eclogae Geol Helv*. 2003;96:451–469. https://doi.org/10.5169/seals-169032.

26. Wild KM, Amann F. Experimental study of the hydro-mechanical response of Opalinus Clay – Part 2: Influence of the stress path on the pore pressure response. *Eng Geol*. 2018;237:92–101. https://doi.org/10.1016/j.enggeo.2018.02.011.
27. Wissa AEZ. Pore Pressure Measurement in Saturated Stiff Soils. *J Soil Mech Found Div*. 1969;95:1063–1074.
28. Witteveen P, Ferrari A, Laloui L. An experimental and constitutive investigation on the chemo-mechanical behaviour of a clay. *Géotechnique*. 2013;63:244–255. https://doi.org/10.1680/geot.SIP13.P.027.